Interferometric sensing of a commercial geophone

OPEN ACCESS
IOP Publishing
Classical and Quantum Gravity
Class. Quantum Grav. **39** (2022) 075023 (11pp) https://doi.org/10.1088/1361-6382/ac595c

Interferometric sensing of a commercial geophone

S J Cooper[1,*], C J Collins[2], L Prokhorov[1], J Warner[3,4], D Hoyland[1] and C M Mow-Lowry[5]

[1] Institute for Gravitational Wave Astronomy, University of Birmingham, Birmingham, B15 2TT, United Kingdom
[2] Department of Physics, University of Maryland, College Park, MD 20742, United States of America
[3] LIGO Hanford Observatory, Richland, WA 99352, United States of America
[4] LIGO Laboratory, California Institute of Technology, Pasadena, CA 91125, United States of America
[5] Vrije Universiteit Amsterdam, 1081 HV, Amsterdam, The Netherlands

E-mail: scooper@star.sr.bham.ac.uk

Received 7 September 2021, revised 28 January 2022
Accepted for publication 28 February 2022
Published 17 March 2022

Abstract

We present a modified commercial L-4C geophone with interferometric readout that demonstrates a resolution 60 times lower than the included coil-magnet readout at low frequencies. The intended application for the modified sensor is in vibration isolation platforms that require improved performance at frequencies lower than 1 Hz. To illustrate it's application a controls- and noise-model of an Advanced LIGO 'HAM-ISI' vibration isolation system was developed, and shows that our sensor can reduce the residual motion of the platforms by a factor of 70 at 0.1 Hz.

Keywords: interferometry, inertial sensing, homodyne detection

(Some figures may appear in colour only in the online journal)

*Author to whom any correspondence should be addressed.

1. Introduction

With the completion of its first three observing runs the Advanced Laser Interferometer Gravitational-Wave Observatory (LIGO) [1] has made incredible advancements in the field of astrophysics, with two highlights being the first direct detections of gravitational waves [2] and merging neutron stars heralding a new era of multi-messenger astronomy [3, 4].

To isolate the test masses from ground motion, LIGO uses a complex system of passive [5, 6] and active isolation [7]. The active isolation is largely provided by the internal seismic isolation (ISI) platforms, that reduce low-frequency motion and holds the in-vacuum optical benches at the correct position and orientation. Despite the success of these systems, the lowest frequencies in the LIGO detection band, 10–20 Hz, are limited by technical noise sources that are in turn caused by residual motion at even lower frequencies [8, 9].

This residual motion must be reduced in order to detect gravitational waves at frequencies as low as 10 Hz [10].

The ISIs are sensed by a mixture of displacement sensors, geophones, and force feedback seismometers. The instrument outputs are 'blended' or 'fused' together to use the best instrument in each frequency band. Two different models of commercial geophones, the Sercel L-4C and Geotech GS-13, are used throughout the detector to measure both the ground motion and the motion of the isolated platforms. While the performance of force feedback seismometers (Nanometrics T240 and Streckeisen STS-2) is inherently superior to that of geophones at frequencies below 0.5 Hz, they are considerably more expensive. As such, only the most critical isolation platforms that house the primary test-masses and beamsplitter use broadband seismometers. Other chambers that house the auxiliary optics must rely on geophones to provide inertial platform measurements.

Coil-magnet geophones are limited by their intrinsic readout noise, caused by the Johnson noise in the geophone coils [11]. The other intrinsic noise source, suspension thermal noise, is around a factor of 200 lower at 10 mHz. With a sufficiently low-noise readout mechanism, the resolution of these sensors can be substantially improved at low frequencies. In the past interferometers have been used to decrease the readout noise contribution in broadband seismometers [12, 13] and thus increase the resolution of these devices. In an earlier paper we constructed a displacement sensor with self-noise low enough to measure suspension thermal noise from 10 mHz to 2 Hz [14].

Improvements to the resolution of geophones will in turn allow for a re-design of the seismic isolation system's blending filters and control loops, substantially reducing sensor noise injection. In particular, they will allow for much improved inertial isolation between 0.1 and 0.3 Hz and reduce the velocity of the platform at critical frequencies.

In this paper we present a fibre-coupled interferometrically sensed L-4C that operates close to suspension thermal noise limit and has 60 times lower self-noise at 10 mHz than the unmodified instrument.

2. Construction of devices

Geophones are devices that measure seismic motion, they are comprised of a sensor coil surrounding a permanent magnet. Either the coil or magnet is attached to a suspended mass, while the other is attached to the device's housing. Depending on the specific instrument the order of these two components can be reversed. Above the sensors resonance frequency the coil connected to the spring is inertially still and the magnet moves according to the input ground motion. This motion between the coil and spring generates a proportional voltage that can be measured and converted back into velocity, displacement or acceleration as appropriate. At

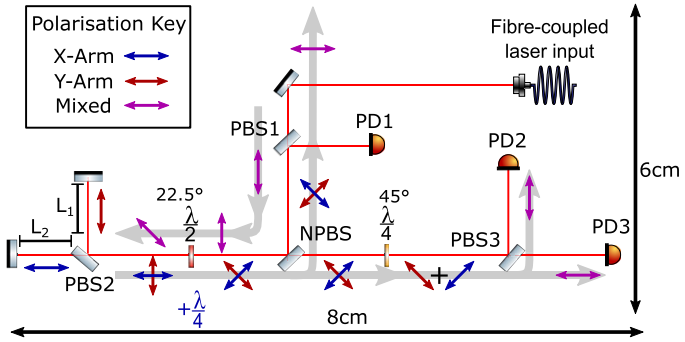

Figure 1. The layout of HoQI used as an interferometric readout on the modified L-4C.

frequencies below their fundamental mechanical resonance, they are increasingly insensitive due to the reduction in relative motion between the magnet and coil. The displacement response of this signal is proportional to the square of the frequency below its resonance, while many of the noise terms remain roughly constant or increase at low frequencies.

To recover the input ground motion below resonance, the signal must be multiplied (in the frequency domain) by the inverse of the geophone's mechanical response, a process often called plant inversion. The inverse response P^{-1} is given by the equation,

$$P^{-1} = \frac{-\omega^2 + \frac{i\omega\omega_0}{Q} + \omega_0^2}{\omega^2}, \tag{1}$$

where ω is the angular frequency, and ω_0 and Q are the (angular) resonant frequency and quality factor of the proof-mass' mechanical resonance. Plant-inversion correctly re-shapes the signal, but noise terms increase rapidly at low-frequencies compared to the measured signal, and the resulting output for typical levels of ground motion is dominated by self-noise below approximately 0.1 Hz for the L-4C.

To integrate the interferometric readout with the L-4C the outer can of each geophone was removed to gain access to the moving proof mass and to prepare the outer can for the attachment of the interferometric readout. Mounting holes were tapped and a large hole in the outer can was milled to allow the attachment of a light-weighted mirror mount to readout the motion of the proof mass.

The interferometer used to measure the L-4C is an upgraded version of the HOmodyne Quadrature Interferometer (HoQI) sensor presented in [14]. A schematic of the optical layout of this device is shown in figure 1. The input laser light is injected into the interferometer through a single-mode polarisation-maintaining fibre. The beam is steered by a 45 degree mirror before being transmitted through a polarising beamsplitter to maximise the purity of the interferometer input polarisation, improving on the previous design by reducing the amplitude of spurious interferometers and increasing fringe visibility. The input alignment is handled by a custom mount for the collimator which is adjusted such that the laser light strikes the test mirror and returns to the photodiodes. The reference beam is then aligned to overlap with the test beam using a half-inch vacuum-compatible kinematic mount, thereby maximizing the fringe visibility at the interferometer readout.

The device features an optical baseplate measuring 8 $\times$ 6 cm that was rigidly attached to the outer can of the L-4C using three M2 bolts. Improving the coherence between multiple interferometric L-4Cs drove several design changes. We used a more stable fibre coupler, and

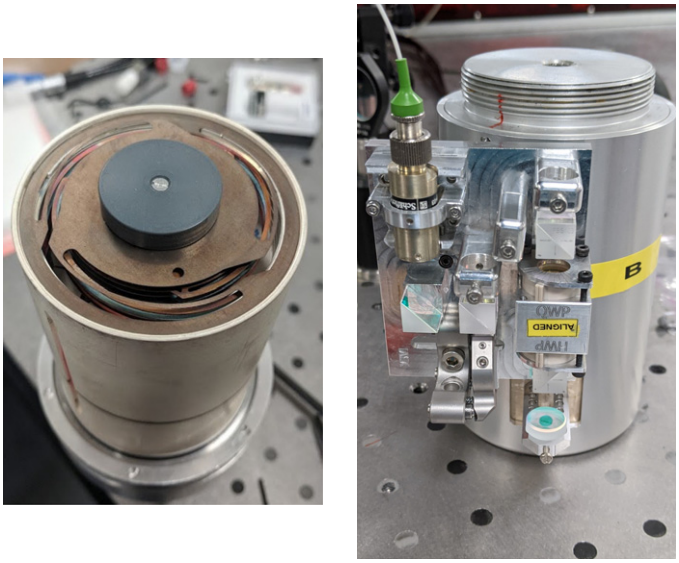

Figure 2. (a) Image showing the internal leaf springs of the L-4C during modification. (b) Prototype version of HoQI used as a readout for an inertial sensor. The baseplate measures 8 × 6 cm and is fixed to the side of an L-4C geophone.

improved waveplate and beamsplitter mounting structure resulting in approximately a factor 10 more coherence between adjacent sensors. An image of the prototype device is shown in figure 2.

The length of the reference arm was adjusted to match the length of the readout arm to better than 1 mm when the moving mass is at rest, minimising frequency noise coupling. The compactness of the device and its side mounting allows us to continue use the geophone coil-readout in parallel, providing a linear, calibrated, and high-coherence verification signal during operation.

3. Noise sources

The main noise sources for the interferometric L-4C are suspension thermal noise, readout noise, and laser frequency noise. The suspension thermal noise is calculated using the properties of the L-4C, this has a resonant frequency of 1 Hz, a quality factor of 2.5 and a mass of 1 kg. The equations given by Saulson [15] are propagated through the plant, as shown in [16]. The thermal noise is then given by the equation,

$$X_{g,\mathrm{th}} = \sqrt{4k_{\mathrm{B}}Tm\omega_0^2\frac{\phi}{\omega}}\frac{1}{m\omega^2}, \tag{2}$$

where $X_{g,\mathrm{th}}$ is the thermal noise, m is the mass, ϕ is the loss angle, T is the temperature and ω_0 is the resonance frequency of the inertial sensor.

Another source of readout noise is the laser frequency noise, and can be calculated using the equation,

$$\delta L = \frac{L\delta f}{f_0}, \tag{3}$$

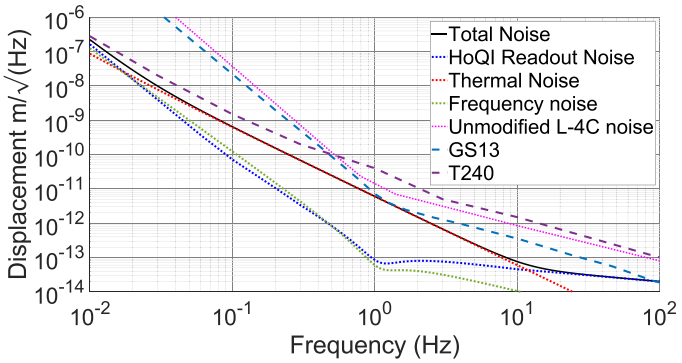

Figure 3. A noise budget of the optical inertial sensor. The interferometer readout noise (blue), structural thermal noise (red) and frequency noise (green) are summed in quadrature to produce the expected resolution of the optical L-4C (black). For comparison the resolution of an L-4C with coil readout is shown in magenta, the GS13 shown in dashed blue and the T240 in dashed purple.

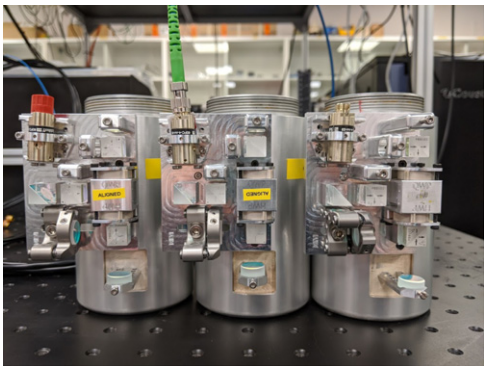

Figure 4. A photo of the three modified interferometric L-4Cs before they were huddle tested.

where L is the length mismatch between the two arms, f_0 is the (optical) frequency of the laser and δf is the laser frequency noise. To minimise the input laser frequency fluctuations we used a 1064 nm solid-state Innolight Mephisto 500NE laser which has frequency noise of $\sim 10^5$ Hz Hz$^{-1/2}$ at 0.1 Hz and our interferometer had an arm length mismatch of 1 mm.

The readout noise trace is based on the sensitivity curve presented in [14], which was measured with an smaller effective path length difference of 0.7 mm. Both the laser frequency noise and readout noise are filtered by the plant-inversion filter of the L-4C from equation (1). This readout noise trace itself is comprised of frequency noise, laser intensity noise and birefringence noise. The latter of these is not well quantified due to the range of quality of optical components, chapter 2 [17]. Noise due to the electronics has previously been calculated and is an order of magnitude lower than these other noise sources.

A noise budget highlighting the dominant noise sources is shown in figure 3.

Below 20 mHz the device will be limited by frequency noise coupling, as this has a f^{-3} dependency below the resonant frequency of the L-4C. In future instruments this can be reduced by either minimising the length mismatch between the two arms or stabilizing the laser frequency. At 10 mHz frequency noise is predicted to be only a factor of 2–3 higher than

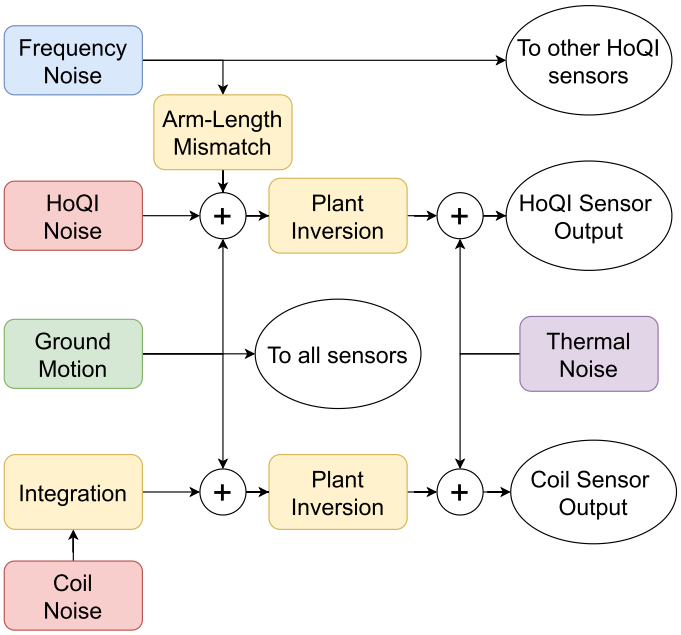

Figure 5. A block diagram illustrating different noise sources present in the device. Uncorrelated noises that cannot be suppressed using a huddle test are shown in red, correlated motion is shown in green. The frequency noise is common between all HoQI-L4C sensors, while thermal noise is common between the interferometric readouts and coil readouts on an individual sensor but are uncorrelated between multiple sensors.

the suspension thermal noise, so only minimal changes are required in our chosen sensitivity band. Suspension thermal noise limits the resolution of the device between 20 mHz and 10 Hz. At frequencies above 10 Hz readout noise is the only significant source of noise.

To measure the self noise of interferometric L-4Cs the sensors must be isolated from external sources of motion, such as air currents, vibrations, thermal effects, and acoustic noise. The largest of these is seismic motion that is on the order of 1 μm Hz$^{-1/2}$ at approximately 0.15 Hz. While this motion is large, it is coherent between multiple sensors provided that they are placed close together. Kirchhoff [11] showed that the self-noise of a group of sensors could be measured in the presence of a large background signal by performing a huddle test whereby the coherent ground motion is subtracted from the a reference sensor to reveal its self-noise (figure 4).

This technique requires the sensors to have large dynamic range and be close together in order to subtract as much of the large background seismic signal as possible, while still having the precision required to sense the underlying sensor self-noise.

Three L-4Cs utilising interferometric and coil readouts were placed close together and huddle tested inside an insulated box to minimise temperature, acoustic, and air current induced noise. The residual signal from an overnight measurement was processed using a MATLAB script (multi-channel coherence subtraction), developed by Brian Lantz and Wensheng Hua, removing any coherent signal present in the reference sensor(s) from the target sensor. This method is described in more detail by Kirchhoff [11]. A block diagram illustrating the correlated signals which can be suppressed using this technique, and uncorrelated noises which cannot be removed, is shown in figure 5.

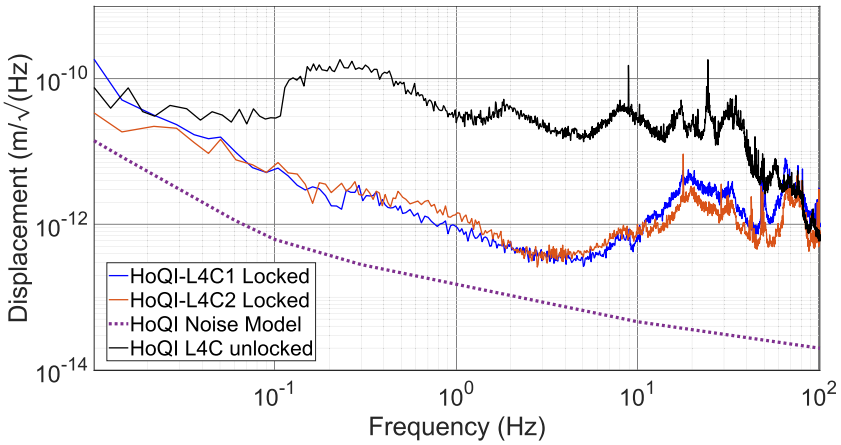

Figure 6. The amplitude spectral density of the displacement measured by HoQI with L-4C mass locked (blue, red). The unlocked interferometer signal with the device exposed to ground motion is shown in black for comparison. In all traces the coherent information has been removed using multiple sensors. The mechanical response of the sensor has not been accounted for and the thermal noise is not included. The expected interferometer noise is shown in dashed purple.

4. Results

Figure 6 shows the raw output of two interferometers mounted onto L-4Cs when the device was placed on the laboratory floor with the mass locked (shown in blue and red) to establish the tested noise floor of the device, the spectrum with the mass unlocked is shown in black for comparison. The red and blue traces represent two HoQI-L4Cs that were placed in an insulated box to minimise temperature gradients and air currents. Coherent motion measured by both devices was removed**.** The black trace is generated by subtracting all common motion measured by two HoQI-L4Cs and two L-4Cs with a coil readout. Below 50 mHz the traces showing the locked and unlocked HoQI-L4Cs signal is within a factor of two of each other, indicating that this is approximately the noise floor of the device. Above this frequency there is a large discrepancy of almost 100 at 0.2 Hz between the two traces as the locked device is no longer measuring the ground motion in the laboratory. This decreases towards higher frequencies, where at approximately 100 Hz the motion is similar. Additional investigation is required to establish what is causing the measured motion to be larger than the expected noise at frequencies below 10 Hz. Additional optical L-4Cs could be constructed to increase suppression from multiple sensors. The motion below 10 Hz is approximately $1/f$ and is not common between the devices. Due to the nature of the interferometer, any polarisation changes in the fibres would result in intensity noise and thus be uncommon between the two devices. Above 10 Hz motion from the lab couples into the two devices differentially, preventing the subtraction reaching it's theoretical noise floor. It is not yet known the coupling mechanism, potential sources include the input optical fibre, which couples laser light from the optical table to the isolated box on the floor, acoustic noise, or the finite rigidity of the HoQI-L4C when locked.

To extract the resolution of the HoQI-L4Cs in the presence of large seismic motion, three L-4Cs with optical and conventional readout were measured simultaneously. One interferometer signal was selected as the 'target' and all coherent information from the remaining signals

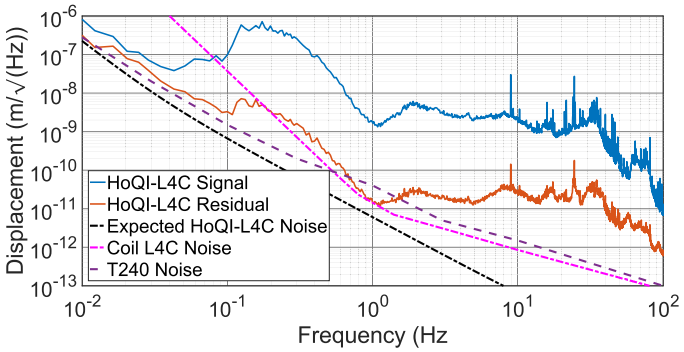

Figure 7. The amplitude spectral density of a HoQI-L4C when exposed to ground motion (blue). Here the measured and predicted resolution of the HoQI-L4C (red, black) with other commercial sensors. The residual signal is generated by subtracting common motion between multiple sensors from a single HoQI-L4C.

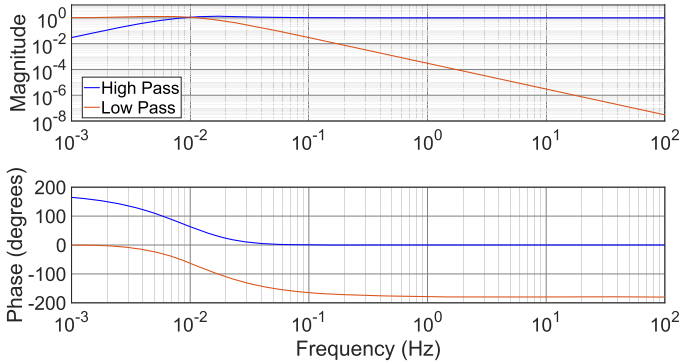

Figure 8. Figure showing the new high and low pass filters generated by optimising equation (4).

was removed to produce traces shown. This residual signal is comprised of that interferometer's sensor noise and the uncorrelated components of residual input vibration, acoustic, and thermal effects.

The measured signal and residual traces are compared with the calculated resolution of the HoQI-L4C sensor and two similar seismometers in figure 7. From 10 to 100 mHz and at 1 Hz the sensor resolution is within a factor of two of the predicted, thermal noise limited, sensor resolution shown in dashed black. Between 0.1 and 1 Hz, the factor of 100 suppression of common motion is insufficient to suppress the large input ground motion caused by the microseismic peak. Above 1 Hz insufficient coherence and vibration isolation prevents the residual motion from reaching the expected sensor resolution.

A driving application for these sensors is for use in the LIGO ISI platforms [7] and other high precision experiments requiring low frequency vibration isolation. The ISI employs multiple vertical and horizontal seismometers and position sensors and blends these signals together to provide optimal control of the isolation platforms. To estimate the isolation performance improvement afforded by HoQI-L4Cs, a detailed numerical model of one of the single stage vibration isolation platforms, the HAM-ISI, was constructed. The detailed workings of the

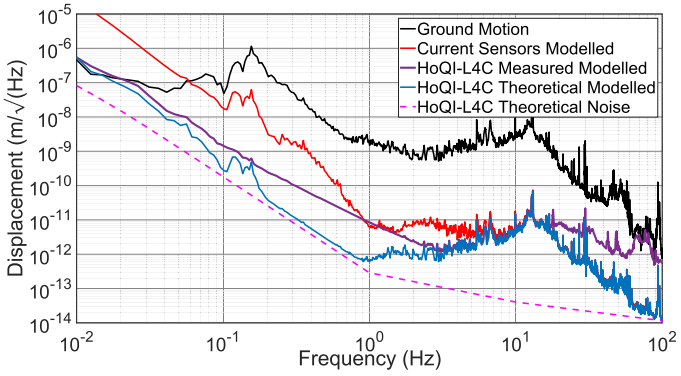

Figure 9. A comparison between the isolation performance using current sensors (red) with the measured and theoretical noise of HoQI-L4Cs (purple and blue respectively). The noise used in the purple and blue traces also include the theoretical suspension thermal noise of the device. The theoretical inertial sensor noise and input ground motion are shown in dashed-magenta and black respectively.

model are outside of the scope of this paper and is detailed in chapter 5 of [17]. The numerical model reconstructs the closed loop performance of the HAM-ISI platform with good fidelity using only inputs from out-of-loop seismometers located near or on the platform's support structures and knowledge of the plant response and loop gains. From these calculations, we can estimate the effects of sensor noise and feedback-control filters.

We subsequently modified the model to include the measured and theoretical HoQI-L4C self-noise in place of the existing GS-13 noise. To take full advantage of the improved sensor noise, new blending filters, shown in figure 8 were generated such that the RMS velocity of the equation,

$$\mathrm{vel}(f) = \mathrm{HP} \times \mathrm{ISNoise} + \mathrm{LP} \times \mathrm{DispNoise}, \tag{4}$$

is minimised. Here HP, LP are the high- and low-pass blending filters and ISNoise and DispNoise are the respective spectral densities of the self-noises of the inertial and displacement sensors. The improvement of low frequency resolution in the HoQI-L4C allows the blending frequency of these filters to be reduced from approximately 250 mHz to 10 mHz.

The model was run using typical seismic input data from the LIGO Hanford site, noise from the HoQI-L4C noise budget, and with the aforementioned blending filters. Existing feedback-control filters were not changed and we do not expect any change in the loop stability. Figure 9 shows a comparison between the estimated platform motion using existing sensors and the new configuration, with an estimated 70-fold reduction in motion at 0.1 Hz and 10-fold reduction at 2 Hz using the theoretical HoQI-L4C trace. It is the reduction in blending frequency that reduces the position sensor noise coupling into the overall motion of the isolation platforms up to 10 Hz where the loop gain is close to unity. This effect is reduced using the measured HoQI-L4C noise (purple), though the estimated motion is still reduced by a factor of 10 at 0.1 Hz and by a factor of 2–5 between 2 and 5 Hz. Above 20 Hz the excess noise in the measured HoQI-L4Cs prevent the purple trace from reaching the performance reached by the current sensors, though this should be treated as an upper limit.

5. Conclusion

In this paper we have detailed the development of an L-4C seismometer that has been adapted to use a high resolution interferometric readout. These modifications increase the resolution of the sensor by factor of 60 at 10 mHz and a factor of 5 at 10 Hz over the unmodified instrument. Through early testing, this resolution has been experimentally verified between 10 and 100 mHz, however residual ground motion has prevented the modified device's resolution being currently verified at higher frequencies. A numerically simulated model of an Advanced LIGO HAM-ISI was created to quantitatively predict the improvement that this could provide in suppression of ground motion, compared to vibration isolation systems currently used in LIGO. This model estimates that interferometrically readout L-4Cs can increase the isolation performance by a factor of 70 at 0.1 Hz and a factor of 10 at 2 Hz.

Acknowledgments

We thank John Bryant for technical support, Maura Shea and Isaac Davis for integration and testing of the data acquisition systems used in this project. The authors acknowledge the support of the Institute for Gravitational Wave Astronomy at the University of Birmingham, STFC 'Astrophysics at the University of Birmingham' Grant ST/S000305/1.

Data availability statement

The data that support the findings of this study are available upon reasonable request from the authors.

ORCID iDs

S J Cooper https://orcid.org/0000-0001-8114-3596
L Prokhorov https://orcid.org/0000-0002-0869-185X
C M Mow-Lowry https://orcid.org/0000-0002-0351-4555

References

[1] Aasi J *et al* 2015 Advanced LIGO *Class. Quantum Grav.* **32** 074001
[2] Abbott B P *et al* 2016 Observation of gravitational waves from a binary black hole merger *Phys. Rev. Lett.* **116** 061102
[3] Abbott B P *et al* 2017 GW170817: observation of gravitational waves from a binary neutron star inspiral *Phys. Rev. Lett.* **119** 161101
[4] Abbott B P *et al* 2017 Multi-messenger observations of a binary neutron star merger *Astrophys. J.* **848** L12
[5] Aston S M *et al* 2012 Update on quadruple suspension design for advanced LIGO *Class. Quantum Grav.* **29** 235004
[6] Cumming A V *et al* 2012 Design and development of the advanced LIGO monolithic fused silica suspension *Class. Quantum Grav.* **29** 035003
[7] Matichard F *et al* 2015 Seismic isolation of advanced LIGO: review of strategy, instrumentation and performance *Class. Quantum Grav.* **32** 185003
[8] Martynov D V 2015 Lock acquisition and sensitivity analysis of advanced LIGO interferometers *PhD Thesis* California Institute of Technology
[9] Martynov D V *et al* 2016 Sensitivity of the advanced LIGO detectors at the beginning of gravitational wave astronomy *Phys. Rev.* D **93** 112004

[10] Yu H *et al* 2018 Prospects for detecting gravitational waves at 5 Hz with ground-based detectors *Phys. Rev. Lett.* **120** 141102
[11] Kirchhoff R *et al* 2017 Huddle test measurement of a near Johnson noise limited geophone *Rev. Sci. Instrum.* **88** 115008
[12] Zumberge M, Berger J, Otero J and Wielandt E 2010 An optical seismometer without force feedback *Bull. Seismol. Soc. Am.* **100** 598–605
[13] Watchi J, Ding B, Matichard F and Collette C 2016 Development of a high-resolution optical inertial sensor for sub-Hz seismic isolation *ISMA Int. Conf. on Noise and Vibration Engineering*
[14] Cooper S J, Collins C J, Green A C, Hoyland D, Speake C C, Freise A and Mow-Lowry C M 2018 A compact, large-range interferometer for precision measurement and inertial sensing *Class. Quantum Grav.* **35** 095007
[15] Saulson P R 1990 Thermal noise in mechanical experiments *Phys. Rev.* D **42** 2437–45
[16] Harms J and Mow-Lowry C M 2017 Suspension-thermal noise in spring-antispring systems for future gravitational-wave detectors *Class. Quantum Grav.* **35** 025008
[17] Cooper S J 2020 Breaking the seismic wall: how to improve gravitational wave detectors at low frequency *PhD Thesis* University of Birmingham